World Journal of Engineering Research
Print ISSN: 2959-9865
Online ISSN: 2959-9873
DOI: https://doi.org/10.61784/wjer3104

PROGRESSIVE MODELING FOR SILICON CARBIDE EPITAXIAL LAYER THICKNESS MEASUREMENT: FROM DUAL-BEAM THEORY TO MULTI-BEAM INTERFERENCE CORRECTION

QiMin Gao[#,*], YiYi Luo[#]
School of Information Science & Engineering, Yunnan University, Kunming 650500, Yunnan, China.
[#]*These authors contributed equally to this work.*
[*]*Corresponding Author: QiMin Gao*

Abstract: Combining infrared reflection interferometry with experimental validation, this paper presents a layered structural modeling and inversion approach for measuring the thickness of silicon carbide (SiC) epitaxial layers. To overcome the challenges in directly acquiring critical parameters during measurement, an analytical relationship between the epitaxial layer thickness and the wavenumber, incident angle, refractive index, and interference order is established. This framework integrates geometric optics, Snell's law, and the Fresnel equations within a dual-beam interferometry context. To handle the discrete and non-uniformly sampled nature of the measured reflectance spectra, the optimal interpolation method is selected based on cross-validation and the root mean square error (RMSE) criterion. Refractive index inversion is subsequently conducted via a golden section search, while the Brent method is employed to accurately locate interference extrema, enabling stable thickness inversion at incident angles of 10° and 15°. Furthermore, recognizing that multi-beam interference (MBI) typically dominates in practical experiments, this study investigates the coherent superposition of multiple reflected beams. A necessary condition for significant MBI ($R^2 \to 1$) is derived, and a comprehensive MBI model—incorporating complex amplitude reflection coefficients and phase correction terms—is developed. This research provides a robust theoretical and mathematical foundation for the high-precision, non-destructive measurement of SiC epitaxial layer thickness.
Keywords: Epitaxial layer thickness; Infrared reflection interferometry; Dual-beam interference; Multi-beam interference (MBI); Inversion algorithm

1 INTRODUCTION

Silicon carbide (SiC) is a pivotal wide-bandgap semiconductor characterized by exceptional physical properties. Crucially, the precision of its epitaxial layer thickness is a primary determinant of device performance, necessitating the development of robust and accurate calculation algorithms. Infrared interferometry, a non-destructive characterization technique, has become the industry standard for such measurements; however, its accuracy remains sensitive to factors including doped carrier concentration and spectral wavelength.

Infrared interferometry exploits interference fringes generated by the reflection and transmission of light within an 'air–epitaxial layer–substrate' structure, applying inverse calculations to the reflectance spectrum to determine layer thickness. Early investigations established the efficacy of this approach, albeit emphasizing its strong dependency on interface phase correction [1]. To mitigate these constraints, a hybrid scheme integrating far-infrared ellipsometry and near-infrared interferometry was subsequently introduced to facilitate measurements across diverse material thicknesses [2]. Furthermore, a fringe-difference fitting model was proposed to enhance inversion stability for homogeneous SiC layers [3]. Recent advancements in computational techniques have shifted the research focus toward the simultaneous inversion of refractive index and thickness. Notable innovations include combining the Cauchy dispersion model with nonlinear least-squares for interference peak order calculation and direct optimization methods [4-5], both of which ensure consistency and high precision across varying incident angles. Concurrently, methodologies utilizing reflectance spectral envelopes and deep learning have demonstrated remarkable success—even under low signal-to-noise ratios—enhancing both measurement precision and noise immunity [6-8]. In practical applications, however, multi-beam interference presents a pervasive challenge, with its severity dictated by reflectance and phase matching [9-10], which ultimately compromises measurement precision [11-12]. To suppress these interference-induced errors, various strategies have been explored, including complex amplitude and phase corrections, precise orientation measurement of interference fringes, and global optimization algorithms [13-17]. Nevertheless, the accuracy and stability of these models remain constrained when applied to complex multi-layer structures or varying material types and thicknesses. Consequently, further refining fringe positioning and thickness inversion algorithms remains a critical bottleneck for high-precision infrared interferometry.

Addressing these gaps, the present study adopts a geometric optics approach to establish an interferometric thickness measurement model that explicitly accounts for refractive index dispersion relative to the incident angle. By designing robust spectral processing and thickness estimation algorithms, this work aims to reconcile the discrepancies between

© By the Author(s) 2026, under the CC BY-NC-ND license (http://creativecommons.org/licenses/by-nc-nd/4.0).

dual-beam and multi-beam interference models, ultimately achieving high-precision, non-destructive characterization of silicon carbide epitaxial layer thickness.

2 METHODOLOGY

2.1 A Dual-beam Interference Model

2.1.1 Theoretical forward model

The measurement of SiC epitaxial layer thickness is based on infrared dual-beam interference. The incident light is split at the top surface and the epilayer-substrate interface, creating an optical path difference proportional to the layer depth, as illustrated in Figure 1.

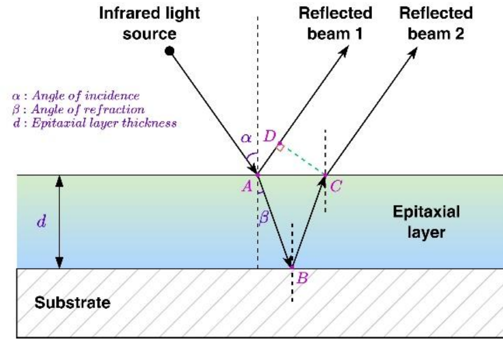

Figure 1 Schematic of Dual-Beam in an Epitaxial Layer

As shown in Figure 1, it can be deduced from the geometric relationships that the distances traveled by reflected beam 1 from point D and reflected beam 2 from point C are identical. Consequently, the geometric path difference between the two beams corresponds to $(l_{AB}+l_{BC})-l_{AD}$.

Furthermore, considering the transition from air (lower refractive index) to the epitaxial layer (higher refractive index), a half-wave loss ($\lambda/2$ phase shift) occurs upon reflection at interface A. Accounting for this phase change, the total optical path difference between reflected beam 1 and reflected beam 2 is expressed as Equation (1):

$$\delta=n_\beta(l_{AB}+l_{BC})-l_{AD}+\frac{\lambda}{2} \tag{1}$$

where δ denotes the optical path difference between reflected beam 1 and reflected beam 2, n_β is the refractive index of the epitaxial layer, and λ represents the wavelength of the infrared light in air.

where denotes the optical path difference between reflected beam 1 and reflected beam 2, is the refractive index of the epitaxial layer, and represents the wavelength of the infrared light in air.

Based on the geometric relationships within a right triangle, l_{AB}, l_{BC}, and l_{AD} can be expressed in the form of Equations (2) and (3):

$$l_{AB}=l_{BC}=\frac{d}{\cos\beta} \tag{2}$$

$$l_{AD}=2d\cdot\tan\beta\cdot\sin\alpha \tag{3}$$

where d represents the epitaxial thickness.

According to Snell's law, the relationship between the refractive index of air (n_α), the refractive index of the epitaxial layer (n_β), the angle of incidence (α), and the angle of refraction (β) is given by Equation (4):

$$n_\alpha\sin\alpha= n_\beta\sin\beta \tag{4}$$

Assuming the refractive index of air is unity, Equation (4) simplifies to Equation (5):

$$\sin\beta=\frac{\sin\alpha}{n_\beta} \tag{5}$$

Based on trigonometric identities, $\cos\beta$ and $\tan\beta$ can be expressed in terms of the incident angle (α) and the refractive index of the epitaxial layer (n_β), as shown in Equations (6) and (7):

$$\cos\beta=\sqrt{1-\frac{\sin^2\alpha}{n_\beta{}^2}}=\frac{\sqrt{n_\beta{}^2-\sin^2\alpha}}{n_\beta} \tag{6}$$

$$\tan\beta=\frac{\sin\alpha}{\sqrt{n_\beta{}^2-\sin^2\alpha}} \tag{7}$$

Substituting Equations (6) and (7) into Equation (3) and simplifying the expression, the final equation for the optical path difference (δ) is obtained as follows:

$$\delta=2d\sqrt{n_\beta{}^2-\sin^2\alpha}+\frac{\lambda}{2} \tag{8}$$

Based on the principle of thin-film interference, the extrema of the interference intensity are determined by the phase relationship governed by δ. The governing equations are given as:
For bright fringes:

$$\delta=2d\sqrt{n_\beta^2\text{-}\sin^2\alpha}+\frac{\lambda}{2}=k\lambda,\ \ k=1,2,3,\ldots \tag{9}$$

For dark fringes:

$$\delta=2d\sqrt{n_\beta^2\text{-}\sin^2\alpha}+\frac{\lambda}{2}=\frac{2k+1}{2}\lambda,\ \ k=1,2,3,\ldots \tag{10}$$

where k denotes the order of interference.
The order k corresponding to the extrema of the interference intensity can be obtained by rearranging Equations (9) and (10), as shown in Equations (11) and (12):
For bright fringes:

$$k=\frac{2d\sqrt{n_\beta^2\text{-}\sin^2\alpha}}{\lambda}+\frac{1}{2} \tag{11}$$

For dark fringes:

$$k=\frac{2d\sqrt{n_\beta^2\text{-}\sin^2\alpha}}{\lambda} \tag{12}$$

From Equations (11) and (12), the order difference between any two extrema—including both bright and dark fringes—can be an integer or a half-integer, represented as $\frac{1}{2},1,\frac{3}{2},2$ and so on. By defining the wavelength of the first observed intensity extremum as the reference, the interference order k_i for the ith extremum is formulated as:

$$k_i=\frac{m_{1i}\lambda_1}{\lambda_1\text{-}\lambda_i}+0.5 \tag{13}$$

where m_{1i} represents the order difference between the ith extremum and reference extremum.
In the context of spectral analysis, the wavenumber ω is defined as the reciprocal of the wavelength, i.e., $\omega=1/\lambda$. By combining Equations (9) through (14), the final expression for the epitaxial layer thickness (d_i) corresponding to the ith extremum is derived in terms of both wavelength and wavenumber as given in Equation (14):

$$d_i=\frac{k_i\lambda_i}{\sqrt{n_\beta^2\text{-}\sin^2\alpha}}+\frac{\lambda_i}{2}=\frac{m_{1i}}{2\sqrt{n_\beta^2\text{-}\sin^2\alpha}}\cdot\frac{1}{\frac{1}{\lambda_i}\text{-}\frac{1}{\lambda_1}}+\frac{\lambda_i}{2}=\frac{m_{1i}}{2\sqrt{n_\beta^2\text{-}\sin^2\alpha}}\cdot\frac{1}{\omega_i\text{-}\omega_1}+\frac{\lambda_i}{2} \tag{14}$$

where d_i denotes the thickness of the epitaxial layer corresponding to the ith extremum and ω_i represents the ith wavenumber of the ith extremum.

2.1.2 Theoretical modeling of reflectance based on fresnel equations

While Equation (14) forms the basis for thickness estimation, the refractive index n_β must be quantified as a prior condition. Drawing upon fundamental principles of wave optics, Fresnel's laws provide a comprehensive framework for describing the amplitude relationships of reflected and transmitted rays at the interface between two media. These equations are universally applicable to a wide spectrum of light waves and form the theoretical basis for analyzing optical interactions. By incorporating parameters such as the incident angle, refractive angle, and the refractive indices of the respective layers, the generalized Fresnel equations allow for the precise determination of the amplitude reflection coefficient at the boundary.
Considering the propagation characteristics of infrared radiation within the air–epitaxial–substrate structure, the incident light is resolved into two orthogonal polarization components. The resulting generalized Fresnel equations are formulated as shown in Equation (15):

$$\begin{cases} r_{//}=\dfrac{n_\beta\cos\alpha\text{-}n_\alpha\cos\beta}{n_\beta\cos\alpha+n_\alpha\cos\beta} \\ r_{\perp}=\dfrac{n_\alpha\cos\alpha\text{-}n_\beta\cos\beta}{n_\alpha\cos\alpha+n_\beta\cos\beta} \end{cases} \tag{15}$$

where $r_{//}$ represents the amplitude reflection coefficient for light incident parallel to the interface, and $r_{\perp}$ denotes the amplitude reflection coefficient for light incident perpendicular to the interface.
The intensity reflectance R is defined as the square of the amplitude reflection coefficient r, i.e., $R=r^2$. By applying Snell's law to eliminate the refraction angle, a direct relationship between the reflectance and the refractive index is established, as expressed in Equation (16):

$$\begin{cases} R_{//}=\left(\frac{n_\alpha\cos\alpha\text{-}n_\beta\cos\beta}{n_\alpha\cos\alpha+n_\beta\cos\beta}\right)^2 \\ R_{\perp}=\left(\frac{n_\alpha\cos\alpha\text{-}n_\beta\cos\beta}{n_\alpha\cos\alpha+n_\beta\cos\beta}\right)^2 \\ \frac{n_\alpha}{n_\beta}=\frac{\sin\beta}{\sin\alpha} \end{cases} \tag{16}$$

Given that the incident infrared radiation is unpolarized (i.e., natural light), the total reflectance R is determined by the arithmetic mean of the parallel and perpendicular polarization components, as given in Equation (17):

$$R=\frac{R_{//}+R_{\perp}}{2} \tag{17}$$

In summary, substituting Equation (16) into (17) allows the refractive index of the outer layer to be determined analytically.

2.1.3 Numerical retrieval of inversion algorithm for refractive index

Based on the mathematical framework established above, the systematic workflow for the proposed numerical inversion is synthesized and summarized in Table 1.

Table 1 The Pseudocode of Refractive Index Inversion

Algorithm 1: Refractive Index Inversion Based on Golden Section Search
Input: Measured reflectance R_{exp}, incident angle θ, Ambient refractive n_0=1.
Output: Target refractive index n^*.
1: **Normalization**
Standardize R_{exp} to [0,1] if necessary.
2: **Internal Reflectivity Model $R(n,\theta)$**
Compute θ_t=arcsin $\left(n_0\sin\frac{\theta}{n}\right)$;
Calculate $R_{//}(n,\theta)$ *and* $R_{\perp}(n,\theta)$ using Fresnel expressions;
return $R=(R_{//}+R_{\perp})/2$.
3: **Optimization and Retrieval**
for each data point do:
if R_{exp} is a boundary value then
Set n^* directly based on physical limits;
else
Solve $n^*=argmin\left\|R(n,\theta)\text{-}R_{exp}\right\|$ within $n\in[1.01,4]$;
if solver fails then execute $n^*=(1+\sqrt{R})/(1\text{-}\sqrt{R})$;
end
4: **Return** the sequence of n^*.

Owing to the transcendental nature of Equations (16) and (17), an analytical closed-form solution for the refractive index n is mathematically inaccessible. Consequently, a numerical inversion scheme is developed to achieve high-precision retrieval. Based on the dielectric constants of Silicon Carbide (SiC) and the physical constraints at the air-medium interface, the optimization domain is bounded within $n\in[1.01,4]$. As detailed in Algorithm 1, a constrained one-dimensional search—specifically the Golden Section strategy—is utilized to minimize the residual between theoretical predictions and experimental observations, thereby ensuring a robust estimation of the target refractive index. This procedure ensures a robust search for the optimal refractive index while strictly adhering to the mandated physical constraints.

2.1.4 Numerical retrieval of epitaxial layer thickness

Following the theoretical framework of interference, this section details the numerical implementation for thickness retrieval as shown in Table 2.

Table 2 The Pseudocode of Epitaxial Layer Thickness Retrieval

Algorithm 2: Epitaxial Layer Thickness Retrieval based on Brent's Method
Input: Wavenumber sequence ω, Reflectance R_{exp}, Refractive index n, Incident angle α.
Output: Predicted thickness d^*.
Initial Parameters:
Define N equal-density intervals across the domain of ω;
Set convergence tolerance $\epsilon=10^{-6}$ and significant threshold δ=0.5.
Extrema Searching (Brent Strategy):
for each interval $[\omega_{start},\omega_{end}]$ do:
Locate local minimum ω_{min} using the Brent method;
Locate local maximum ω_{max} by minimizing the negated function $-R(\omega)$;
Verify peaks/valleys if the local variation exceeds δ and store in $P_{extrema}$
end
Refinement & Sorting:

Sort all detected points $P_i(\omega_i,R_i)$ by wavenumber;
Eliminate duplicate points within a proximity tolerance.
Thickness Calculation (Reference Point Method):
Designate the second extremum (ω_{ref},R_{ref}) as the reference point;
for each extremum P_i ($i\neq ref$) do:
  Determine relative interference order difference m_i;
  Compute instantaneous thickness d_i using Equation (14)
end
return $d^*=\text{mean}(d_i)$ for all $i\neq ref$.

The implementation of Algorithm 2 prioritizes both global convergence and local precision. The use of equal-density interval partitioning ensures that the Brent method effectively captures high-frequency interference fringes without missing local extrema. By selecting the second extremum as a stable reference point, the algorithm mitigates the phase uncertainties inherent in the boundary of the spectrum, thereby reducing the systematic error of the order difference m_i. Finally, the integration of multiple thickness estimations (d_i) through an averaging process provides a statistically robust result that is less sensitive to experimental noise in the reflectance data.

2.2 Multi-Beam Interference (MBI)

2.2.1 Critical conditions for MBI

Building upon the foundational two-beam interference model discussed in the previous section, this section extends the analysis to a more comprehensive multi-beam interference framework. While the two-beam model provides a preliminary approximation, actual infrared reflectance is influenced by infinite internal reflections within the SiC epitaxial layer. To achieve higher precision in characterizing the interferometric spectrum, it is necessary to account for these multiple reflections.

When light reflects back and forth within the epitaxial layer, the phase difference between any given wave and the preceding one corresponds to the zigzag path between the two ends of the plate, as shown in Figure 2:

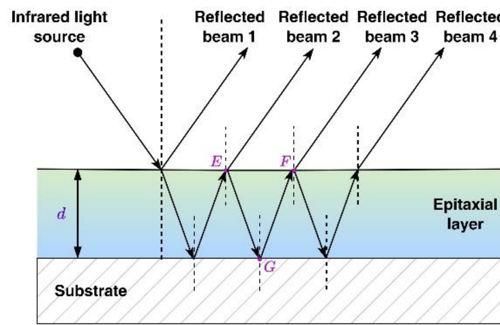

Figure 2 Schematic of Multi-Beam Interference in an Epitaxial Layer

Based on the geometric configuration in Figure 2, the optical path difference (OPD) between two adjacent beams, is determined by the path traveled within the epitaxial layer. In this case, the OPD
between beam 1 and beam equals to $l_{EG}+l_{GF}$. Taking the amplitude of the wave to be a complex number and setting its phase equal to a constant multiple of the phase of the wave function, the OPD can be derived from the formula $\delta=2n_\beta d\cos\theta$ as shown in Equation (18):

$$\delta=\frac{4\pi}{\lambda}n_\beta d\cos\beta \tag{18}$$

Let r_p and $r_p^{'}$ be the reflection coefficients for the incident and reflected waves, with t and $t^{'}$ being the corresponding transmission coefficients. Let $A^{(i)}$ be the amplitude of the electric vector of the incident wave. The complex amplitude of the first reflected beam, i.e. the direct first-order transmission, is $A^{(1)}=tt^{'}A^{(0)}$. For each additional round trip, the amplitude must be multiplied by two reflection coefficients and a phase factor $e^{i\delta}$. Then, according to the recursive relationship,
the amplitude $A^{(p)}$ of the pth reflected wave is expressed as shown in Equation (19):

$$A^{(p)}=tt^{'}\left(r_p r_p^{'}\right)^{p-1}A^{(0)}e^{i(p-1)\delta} \tag{19}$$

The total amplitude A in the direction of transmission is obtained by linearly summing the amplitudes of all reflected light beams, as given in Equation (20):

$$A=\sum_{p=1}^{\infty}A^{(p)}=tt^{'}A^{(0)}\sum_{p=0}^{\infty}(r_p r_p^{'}e^{i\delta})^p \tag{20}$$

Equation (21) is a geometric series with common ratio $q=r_p r_p^{'}e^{i\delta}$. If the absolute value of the common ratio is less than 1, then the series converges.
The relationship between the intensity and amplitude of reflected waves is as follows:

$$I_p \propto \left|A^{(P)}\right|^2 \tag{21}$$

where I_p represents the intensity of the pth reflected wave.

The aggregate effect of multi-beam interference is effectively characterized by the superposition of an infinite sequence of coherent beams, represented mathematically as an infinite series. For this series to yield high-contrast interference patterns, it must fulfill specific convergence criteria; specifically, the terms must not attenuate too rapidly to ensure the resulting fringes maintain sufficient visibility. Therefore, I_{p+1}/I_p should converges to 1. The expression of I_{p+1}/I_p is given by Equation (22):

$$\frac{I_{p+1}}{I_p}=(r_p \cdot r_p^{'})^2 \tag{22}$$

Let R denote the reflectance. Since $R=r^2$, we have:

$$\frac{I_{p+1}}{I_p}=R_p \cdot R_p^{'} \tag{23}$$

where R_p and $R_p^{'}$ respectively denotes the reflectance of top and bottom interface.

Therefore, a necessary condition for significant multi-beam interference to occur is that the square of the reflectance must be very close to unity.

Drawing on the derivation above, we can deduce two significant characteristics:

(i) In the limit where R^2 approaches zero, the ratio I_{p+1}/I_p vanishes to zero. The intensities of the second and subsequent beams become negligible, leading to a rapid convergence of the series. Consequently, the total intensity is dominated by the primary beam, and the system reduces to a regime of two-beam interference.

(ii) Conversely, as R^2 approaches unity, the ratio I_{p+1}/I_p tends toward one. The intensities of all successive beams are comparable to the first, resulting in a very slow convergence of the series. In this case, the contributions of all beams must be taken into account. Their collective interference produces high-finesse, sharp fringes, manifesting as multiple-beam interference.

2.2.2 MBI correction model

As established in Section 2.3.2, reflectivity is a prerequisite for the occurrence of Multiple-Beam Interference (MBI). Unlike dual-beam interference, which involves only two reflected components, the MBI regime consists of a vast number of reflected beams. Consequently, the conventional approach of calculating the total reflectivity for natural light by simply averaging the parallel and perpendicular components is no longer applicable.

In this MBI correction model, the amplitude reflection coefficient is redefined as the ratio of the resultant amplitude of all reflected beams to that of the incident light. Extending the complex amplitude $A^{(i)}$, the phase shift δ between successive beams can be expressed as Equation (24):

$$\delta=2\pi\omega_i n_\beta d_i \cos\beta \tag{24}$$

By introducing the complex phase factor $e^{2i\delta}$, the effective amplitude reflection coefficient $r_{eff,\sigma}$ for each polarization component ($\sigma = \perp$ *or* $//$) is formulated as:s:

$$r_{eff,\sigma}=\frac{r_{p,\sigma}+r_{p,\sigma}^{'}e^{2i\delta}}{1+r_{p,\sigma}r_{p,\sigma}^{'}e^{2i\delta}} \tag{25}$$

It should be noted that while r_{eff} adheres to the law of conservation of energy, it serves primarily as a mathematical construct without direct physical significance. Finally, the relationship between the total power reflectivity R and the effective amplitude coefficient is given by Equation (26):

$$R=\frac{\left|r_{eff,\perp}\right|^2+\left|r_{eff,//}\right|^2}{2} \tag{26}$$

3 RESULTS AND DISCUSSION

3.1 Data Acquisition and Characterization

3.1.1 Data source and description

The experimental datasets analyzed in this study were derived from Problem B of the 2025 China Undergraduate Mathematical Contest in Modeling (CUMCM) [18]. Although the original problem encompasses both silicon carbide (SiC) and silicon (Si) wafers, this research specifically concentrates on the SiC subset (Datasets I & II). These subsets comprise reflectance spectra acquired at incident angles of 10° and 15°, respectively. Each dataset records the wavenumber (expressed in cm^{-1}), against the corresponding reflectance of the interferometric spectrum.

3.1.2 Data analysis and preprocessing

To enhance the dataset and address non-uniform sampling, four candidate interpolation methods were evaluated: Nearest-neighbor, Linear, Cubic Spline, and Piecewise Cubic Hermite Interpolating Polynomial (PCHIP).

The selection was based on the Root Mean Square Error (RMSE) calculated via cross-validation, which is expressed as Equation (27):

$$RMSE = \sqrt{\frac{1}{n}\sum_{i=1}^{n}(y_i-\hat{y}_i)} \tag{27}$$

where n is the number of data points, y_i represents the measured reflectance values and $\hat{y}_i$ denotes the value predicted by the specific interpolation method. The RMSE results for these four methods are summarized in Table 3.

Table 3 The RMSE Values of Four Interpolation Methods

Methods	RMSE values	
	Incident angle = 10° Dataset I	Incident angle = 15° Dataset II
Nearest-neighbor	0.187	0.180
Linear	0.186	0.214
Cubic Spline	0.386	0.442
Piecewise Cubic Hermite	0.387	0.446

As presented in Table 3, the Linear interpolation method outperformed other methods for Dataset I(10°) with an RMSE of 0.186. In contrast the Nearest-neighbor method yielded the minimum RMSE for Dataset II. These optimal methods were applied to Datasets I, II, and the resulting reconstructed spectral curves are presented in Figure 3.

a. Dataset I (10°, Linear) b. Dataset II (15°, Nearest-neighbor)

Figure 3 Spectral Reflectance Curves of Different Datasets Reconstructed by Optimal Interpolation Methods

3.2 Thickness Inversion Based on the Two-Beam Interference Model

Using the golden-section search algorithm described in Section 2.1.3, the refractive index that best matched the experimental reflectance was obtained. The mean optimal refractive index was 2.584 at an incidence angle of 10° and 2.598 at 15°. The relationship between refractive index and reflectance
The distribution of the refractive index is shown in Figure 4:

a. Refractive Index vs. Reflectance b. Refractive Index Distribution

Figure 4 The Results of Refractive Index Calculations for Different Reflectance

In Figure 4(a), the horizontal axis represents the reflectance, and the vertical axis represents the refractive index. The curve generally exhibits a non-linear relationship; when R is less than 0.4, the refractive index increases rapidly with reflectance. When R increases to around 0.4, the refractive index approaches saturation and stabilizes at 4. The experimental data align well with the theoretical curve, indicating that the results obtained using the fminbnd golden

section search for numerical fitting are reliable. Within the actual refractive index range of silicon carbide [2, 3], the corresponding reflectance values are primarily concentrated in the [2, 2.5], which is consistent with the experimentally measured data. In Figure 4(b), the Magenta (incident angle = 10°) and blue (incident angle = 15°) histograms largely overlap, indicating excellent consistency in the refractive index distributions obtained at different incident angles. The main distribution peaks are concentrated in the [2.5, 2.6] range, which aligns with the known physical properties of silicon carbide, where the refractive index lies between 2 and 3.
The extrema were identified using the Brent algorithm in Section 2.1.4, as shown in Figure 5.

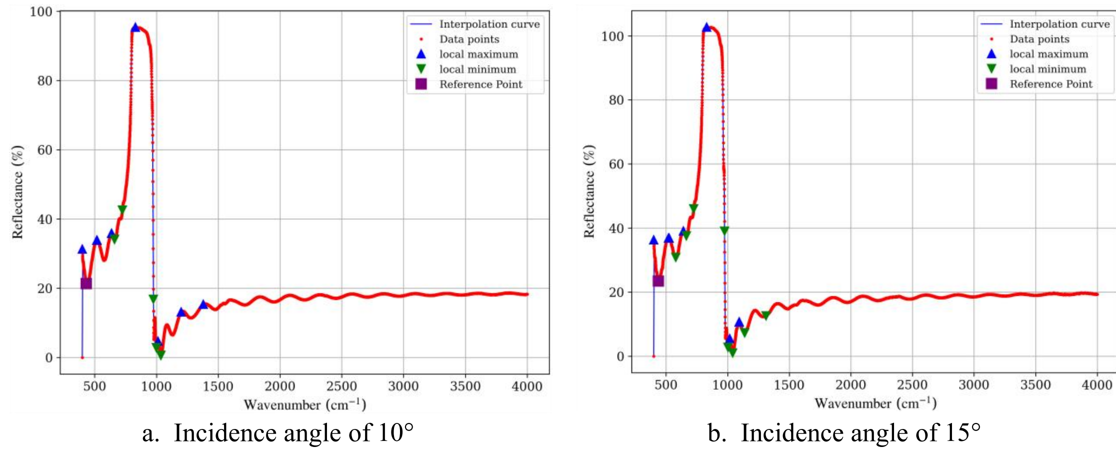

a. Incidence angle of 10° b. Incidence angle of 15°

Figure 5 Reflection Spectra with Selected Local Maxima and Minima for Thickness Estimation

As shown in Figure 5, the first local extremum is clearly the second data point in the graph; however, due to the significant data gap between the first and second data points, the first local extremum is rather unstable. Therefore, the second local extremum is selected in place of the first as the reference point to avoid the issue of instability in the local extrema. The curve in the left-hand figure exhibits a distinct peak in the wavenumber range of 800~1000 cm^{-1}, with a reflectance approaching 100%, rising rapidly to a peak before dropping sharply. Beyond 1000 cm^{-1},the reflectance drops significantly and exhibits periodic oscillations, with the amplitude gradually decreasing. The red smoothed curve, obtained through interpolation, largely coincides with the original data points on the blue line, indicating that the interpolation and extreme point extraction methods are appropriate.
By substituting the obtained refractive indices into Equation (15) together with the extrema calculated by the Brent algorithm, the epitaxial-layer thickness of SiC was as follow:
(i) At an incidence angle of 10°, the average epitaxial layer thickness is 6.7554±2.3301 μm;
(ii) At an incidence angle of 15°, the average epitaxial layer thickness is 6.7066±2.4732 μm.
Both of the calculations excluded the reference point in both cases.

3.3 Thickness Inversion Based on the Multiple-Beam Interference Model

Assuming that multi-beam interference is present in the test results in Dataset 1 and Dataset 2, First, the corrected average refractive index for Dataset 1 was calculated to be 2.236, and the corrected average refractive index for Dataset 2 was calculated to be 2.212. The distribution of the corrected refractive indices is shown in Figure 6.

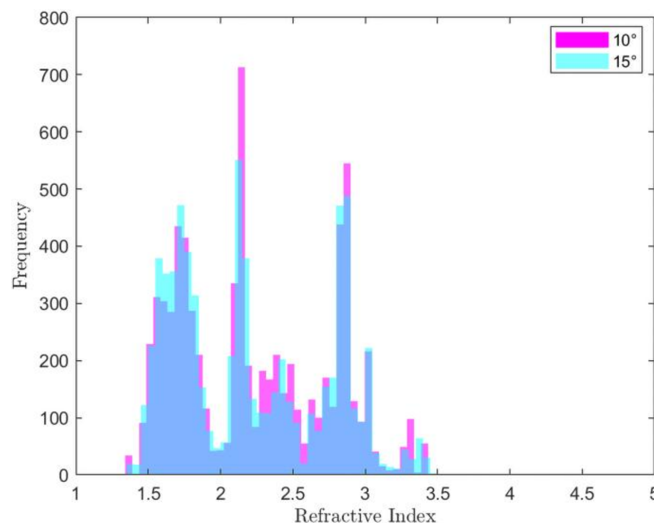

Figure 6 Refractive Index Distribution Corrected Using a Multi-Beam Interference Model

As can be seen from Figure 6, the histograms for the two cases show a high degree of overlap, indicating that the refractive index distributions obtained for Dataset 1 and Dataset 2 following correction using the reflection model are relatively similar.
Thus, the thickness of the SiC epitaxial layer calculated using the reflection correction model in Section 2.2 is as follows:
(i) At an incidence angle of 10°, the average epitaxial layer thickness is 6.7557±2.3301 μm;
(ii) At an incidence angle of 15°, the average epitaxial layer thickness is 6.7065±2.4722 μm.
Both of the calculations excluded the reference point in both cases.

3.4 Comparison and Statistical Validation

A comparison of the results obtained from the two models revealed a deviation of less than 0.1%; it is therefore concluded that the effect of multi-beam interference on the test results of Annexes 1 and 2 is negligible.
A 95% confidence interval analysis was performed for the epitaxial layer thickness. For an incidence angle of 10°, the interval was estimated to be $[5.5138, 7.9970]\,\mu m$, with a width of $2.4832\,\mu m$, corresponding to a relative uncertainty of ±18.38%. For an incidence angle of 15°, the interval was $[5.5491, 7.8410]\,\mu m$, with a width of $2.3150\,\mu m$, corresponding to a relative uncertainty of ±17.26%.

4 CONCLUSION

This research provides a comprehensive solution for the non-destructive measurement of silicon carbide (SiC) epitaxial layer thickness using infrared interferometry. By establishing a hierarchical framework that progresses from a fundamental dual-beam interference model to a refined multi-beam interference (MBI) correction model, and integrating techniques such as spectral interpolation, refractive index inversion, and precise extrema localization, a stable and accurate thickness retrieval is achieved. Grounded in geometric optics, Snell's law, and the Fresnel equations, the proposed algorithm ensures both theoretical consistency and computational efficiency. Notably, the model's ability to identify and mitigate MBI-induced deviations significantly enhances measurement reliability, particularly under high-reflectivity conditions.
Future research will focus on enhancing model fidelity by incorporating complex physical factors such as material dispersion and interface roughness. Simultaneously, the experimental dataset will be expanded with diverse device samples to further validate the model's generalization capability and industrial applicability.

COMPETING INTERESTS

The authors have no relevant financial or non-financial interests to disclose.

REFERENCES

[1] Severin P J. On the infrared thickness measurement of epitaxially grown silicon layers. Applied Optics, 1970, 9(10): 2381-2387.
[2] DeNicola R O, Saifi M A, Frazee R E. Epitaxial layer thickness measurement by far infrared ellipsometry. Applied Optics, 1972, 11(11): 2534-2539.
[3] Zhi-Yun L, Ji-Wei S, Yu-Ming Z, et al. Methods for thickness determination of SiC homoepilayers by using infrared reflectance spectroscopy. Chinese Physics Letters, 2010, 27(6): 068103.
[4] Alharshan G A, Uosif M A M, Emam-Ismail M, et al. A simple new method for retrieving spectral changes of the refractive index of thin films from transmission spectra. Optical Materials, 2023, 146: 114584.
[5] Zhang Y, Zhou Y, Cao Y, et al. Direct optimal calculation method for obtaining the thickness and complex refractive index of chalcogenide glass films. Applied Physics B, 2025, 131(8): 163.
[6] Tchenka A, Agdad A, Ech-Chamikh E. Determination of the thickness and optical properties by reflectance method. Infrared Physics & Technology, 2024, 137: 105117.
[7] Cheng X, Tang Y, Yang K, et al. Deep learning for thin film thickness measurement in spectroscopic reflectometry. IEEE Photonics Technology Letters, 2022, 34(18): 969-972.
[8] Sun J, Li Z, Zhang H, et al. An improved method for measuring epi-wafer thickness based on the infrared interference principle: Addressing interference quality and multiple interferences in double-layer structures. Results in Physics, 2023, 54: 107146.
[9] Zhen-Hua Y, Hui-Hao L, Jin-Dong W, et al. Recent hotspots and innovative trends of infrared photon detectors. Journal of Infrared and Millimeter Waves, 2022, 41(1): 1-25.
[10] Shao J, Chen X, Wang M, et al. Infrared-modulated photoluminescence spectroscopy: From wide-band coverage to micro-area and high-throughput scanning imaging. Acta Physica Sinica, 2025, 74(1).
[11] Fushun Y, Xiaojun D, Qingyan L I, et al. Research on silicon carbide epitaxial equipment technology. Electric Drive for Locomotives, 2023 (5): 191-197.
[12] Chen L, Weitong L, Qiangying X, et al. Research on epitaxial growth of InAs/GaInSb long-wave infrared superlattice materials. Journal of Infrared and Millimeter Waves, 2026, 45(2): 195-206.
[13] Li Y, Jiang S, Chen X, et al. Accurate measurement and adjustment method for interference fringe direction in a scanning beam interference lithography system. Optics Express, 2023, 31(17): 28145-28160.

[14] Kim D W, Kwon M, Park S, et al. Measurement of the thickness and refractive index of a thin film by analyzing reflected interference fringes. Applied Optics, 2023, 62(30): 8018-8024.
[15] He D, Zhang Z, Deng J. Multi-beam interference in GaN epitaxial layer thickness measurement: impact analysis and method optimization. Semiconductor Science and Technology, 2026.
[16] Park J, Cho Y J, Chegal W, et al. A review of thin-film thickness measurements using optical methods. International Journal of Precision Engineering and Manufacturing, 2024, 25(8): 1725-1737.
[17] Yang S, Wang Z, Han X, et al. Accurate infrared interferometric thickness measurement of Silicon carbide epitaxial layers using dynamic refractive index correction. Nondestructive Testing and Evaluation, 2026: 1-26.
[18] Chinese Society for Industrial and Applied Mathematics. 2025 CUMCM Problem B: Determination of silicon carbide epitaxial layer thickness. (2025-09-04) [2026-04-18]. https://www.mcm.edu.cn/html_cn/node/03c91a444e62eee81a3740fa97a461a6.html.